Photogrammetric monitoring of load-induced vertical deformations in the superstructure of a research bridge

Robert Blaskow, Hannes Sardemann, Hans-Gerd Maas
Institute of Photogrammetry and Remote Sensing, TUD Dresden University of Technology, Germany
(robert.blaskow, hannes.sardemann, hans-gerd.maas)@tu-dresden.de

Keywords: Bridge inspection, deformation tracking, structural health monitoring

Abstract

Structural health monitoring of bridge infrastructure is conventionally carried out either through the acquisition of data from embedded sensor arrays or through systematic inspection and documentation of surface-observable changes on the structure. External deterioration, such as crack formation or load-induced structural deformations, is typically identified during these inspections. However, conventional visual inspections are often labor-intensive and costly. Automated, camera-based photogrammetric monitoring methods offer a promising alternative to reduce both effort and expense. For the specific task of detecting vertical deformations in a bridge superstructure, a tripod-stabilized mono camera setup can be utilized. This approach enables the derivation of vertical deformations by tracking the displacement of target points within a predefined measurement field over time.

This study investigates the derivation of vertical deformations from image sequences. Using a representative test bridge as a case study, the characteristic vertical deformation response induced by the traversal of a loaded vehicle is analyzed and documented. A measurement point field was affixed to the bridge superstructure and continuously observed. From the acquired image sequences, continuous vertical displacements were successfully derived, with a mean vertical deflection of the bridge superstructure in the range of −1.71 mm to +0.72 mm. The mean measurement noise, averaged across all monitored test cycles, amounted to 0.01 mm. The results demonstrate that high-quality deformation data can be acquired in a cost-efficient manner using a consumer-grade camera in conjunction with a standardized measurement field, thereby offering a viable low-cost alternative to conventional structural monitoring instrumentation.

1. Introduction

Germany has an estimated total of approximately 130,000 bridge structures, with about 40,000 located within the federal highway network. According to various reports, approximately 16,000 of these bridges are in a state of deterioration or require urgent repair. The poor condition of many bridges is due to several factors, including high traffic loads, the bridges' advanced age, and construction deficiencies. As bridges age, the importance of early detection of structural defects increases. Timely identification of damages enables specific examinations that can significantly reduce the deterioration process and extend the structures' service life. However, given the large number of bridges, relying solely on extensive visual inspections is neither feasible nor efficient. Instead, the implementation of intelligent real-time monitoring systems is essential. These systems continuously collect, aggregate, and analyze data to identify damage indicators. When anomalies are detected, such systems can trigger alarms, allowing for prompt and targeted maintenance measures to address specific issues, thereby ensuring the safety and functionality of the infrastructure.

As part of the DFG (German Research Foundation) priority programme SPP100+, such monitoring systems are being developed based on a digital twin of a bridge structure. In addition to traditional civil engineering sensor technology, image-based photogrammetric methods are employed to monitor the condition of structures. A presentation of the general workflow for the automated creation of semantic-aware geometric as-is models of bridges is given in Kellner et al. (2024).

Load tests are an essential method for obtaining structural health data. These tests are employed to evaluate the load-bearing capacity of existing bridge structures and to conduct material performance assessments under controlled laboratory conditions. Photogrammetric methods are well-established techniques for assessing the condition of concrete structures during these tests. These methods enable precise detection and measurement of deformations in concrete components, as well as the identification of surface-level cracks. The application of photogrammetry in such contexts involves capturing high-resolution images of concrete specimen under load to determine the components of 3D crack opening vectors (Liebold et al., 2020). Another method uses image sequences with an ultrahigh temporal resolution and frame rates exceeding one million frames per second to perform high dynamic material analysis. Duran Vergara et al. (2025) showed the determination of the longitudinal wave propagation velocity and the induced longitudinal deformations from image data of an ultrahigh-speed camera. Koschitzki et al. (2011) showed how deformations and cracks can be identified with a high level of accuracy during a load test in a laboratory setting. Photogrammetrically monitored load tests can be conducted in various settings, including laboratory experiments on model components, in-situ tests on existing bridge structures, or on research bridges. These tests differ primarily in the configuration of the camera systems (e.g., mono-camera or multi-camera setups) and the demonstrators used.

Particularly, the research bridge as an experimental environment offers a significant advantage and is becoming increasingly important in the development of new sensor technology and measurement methods. As well as testing innovative construction methods, sensors can be incorporated deep within the structure during construction. For instance, they can be placed in the reinforcement area. Furthermore, test bridges offer the advantage of an undamaged initial state, which cannot be replicated with real structures in use. Conversely, suitable sensor technology can be used to create a highly controlled measurement environment that includes all atmospheric and meteorological measurement

https://doi.org/10.5194/isprs-archives-XLIX-B2-2026-1139-2026

systems. This is why research bridges are also referred to as real-world laboratories.

Recent studies evaluated the potential of photogrammetric bridge monitoring methods using terrestrial and UAV-based cameras. Albert et al. (2002) showed the results of two pilot studies on detecting vertical bridge deformation measurement by use of a single camera setup in a laboratory and real-world environment. In this study, natural surface patterns were used in addition to artificial targets as reference points, and an image measurement accuracy in the order of 1/100 pixel could be validated. Marendic et al. (2025) illustrates the potential of photogrammetric methods for determining structural displacements during a load test on a real bridge beam.

As well as terrestrial cameras, image sequences captured by unmanned aerial vehicles (UAVs) can be used to determine deformations in bridge superstructures. Maboudi et al. (2025), for instance, developed an UAV-based approach for structural health monitoring as part of the SPP100+, with a focus on detecting geometric deformations of a test bridge under different loads.

This publication presents a scalable and cost-efficient method for monitoring load-induced vertical deformations in real-world bridge superstructures using image sequences. The experiments were carried out in a controlled real-world laboratory environment. To achieve this, a measurement field composed of coded permanent markers was affixed to a bridge span and monitored with a standard camera setup. These investigations were conducted on a full-scale research bridge which is part of the IDA-KI project. (IDA-KI, 2025).

The article is structured as follows. First, the study area (Sec. 2.1), the measurement setup (Sec. 2.2) and the data acquisition (Sec. 2.3) are presented. This is followed by a detailed presentation of the applied photogrammetric method (Sec. 3) and the derived results (Sec. 4). Finally, the article concludes with a discussion of the results and provides an outlook on potential future adaptions (Sec. 5).

2. Study Area and Data Acquisition

2.1 Research Bridge (openLAB) as a Study Area

The openLAB research bridge of the IDA-KI project was constructed and equipped with a civil engineering monitoring system to gather real-world monitoring data and analyze real-life damage scenarios. It is a three-span, prestressed concrete bridge, that has a total length of 45 m and a width of 4.5 m (Figure 1).

Figure 1. IDA-KI openLAB research bridge with load vehicle.

Spans 1 and 2 each comprise three 1.5 m-wide precast elements with a T-beam cross-section and a classic composite panel built with in-situ concrete (Figure 2b). Span 3 consists of precast elements (Figure 2c) from a rapid construction system that does not use in-situ concrete complement (Herbers et al., 2024). A set of rails has been laid across the entire bridge superstructure to enable regular load tests with a load vehicle to be carried out (Figure 2a). A motorized trolley allows loads of different sizes to be moved across the structure on the rails.

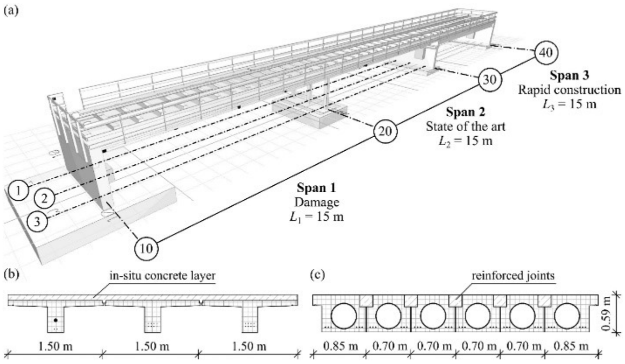

Figure 2. Components and dimensions of the openLAB research bridge. Image source: (Jansen et al., 2025)

The civil engineering monitoring system installed on the research bridge tracks structural conditions and detects damage by identifying changes in the bridge’s state. The system is divided into three categories: global measurements such as inclination, and atmospheric parameters; point-based, location-specific measurements such as concrete or steel strain and joint opening; and line-based, location-specific measurements such as concrete or steel strain. Point measurements are carried out using strain gauges and inductive displacement transducers. These serve several purposes. One of them is to verify the linear measurements carried out using distributed fiber optic sensors (DFOS). The advantage of these DFOS is that, unlike for point measurements, the location of the damage does not need to be known.

The bridge undergoes several phases over the period of the project. These can be broadly categorized as a run-in or reference phase, during which the structure is subjected to regular loads to simulate normal use, and a test phase, during which targeted loads are gradually applied up to and beyond the limit of the structure's load-bearing capacity.

During the reference phase of the bridge, the load vehicle is driven across the bridge at consistent intervals. Here, the load vehicle moves at a constant speed of 4 km/h, starting at bridge span 3 and continuing over span 2 to the end of bridge span 1. It stops near the abutment and returns to its starting position on span 3. This procedure forms one test cycle. For this publication, three load test cycles, monitored at one test day, were used for this purpose. These were conducted on a test when the load vehicle had a current total weight of 1.4 t.

Thanks to the collaboration between the SPP100+ priority programme and the IDA-KI project, the research bridge could be utilized to develop the method presented here for monitoring load-induced vertical deformations in bridge superstructures.

2.2 Photogrammetric Measurement Setup

To monitor vertical deformation, two fields of measurement points, composed of suitable permanent marker for photogrammetric measurements, were installed on the outer spans of the bridge superstructure.

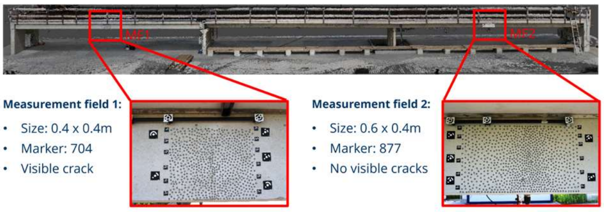

Figure 3. Installed photogrammetric measurement fields and their locations on the openLAB bridge.

One measurement field, comprising 877 markers, was positioned at bridge span 1 (Figure 3 right), and the other, consisting of 704 markers, at span 3 (Figure 3 left). For the purposes of this article, the measurement field 2 at span 1 is the primary focus. These fields were placed as centrally as possible within the spans, as this is where the highest deformation and potential damage were expected.

The measurement targets used in these fields were designed to be highly resistant to external environmental factors, including extreme temperature fluctuations, moisture, and UV radiation. Both coded and uncoded circular targets were employed to ensure robust data acquisition. Due to spatial constraints, the measurement fields were approximately 0.4 m in height, with widths varying between 0.4 m and 0.6 m (Figure 4).

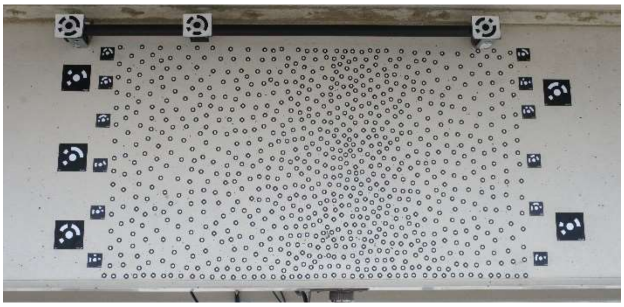

Figure 4. Detailed view of measurement field 2 (MF2).

The high density of uncoded measurement marks, ranging between 704 and 877 per field, facilitates the detection of cracks. Benning et al. (2004) showed the high accuracy potential of photogrammetry using a target grid for monitoring crack origin and evolution of concrete elements. However, crack detection is beyond the scope of this article. For the analysis of the deformation of the bridge superstructure presented here, the coded targets positioned along the edges of the measurement fields were utilized (Figure 4). These coded targets provide precise reference points for tracking deformation.

As different measurements were conducted during the several research phases, changes in the bridge structure due to permanent loads made it impossible to assume stable test fields throughout the monitoring period. To address this, the test fields have to be zero-measured prior to the particular measurement campaign. This process was carried out using a Nikon D300 high-quality SLR camera, ensuring accurate initial data for each measurement cycle.

The image data used for deformation monitoring was acquired using various consumer-grade cameras mounted on tripods. For the data presented in this article, a Nikon Z6 camera was used, equipped with fixed focal length lenses of 50 mm and 35 mm. This setup ensured high-quality image capture, suitable for precise deformation tracking.

2.3 Measurement Data Acquisition

The image data acquisition process was conducted during one load test day. Prior to the load vehicle test cycles, an on-site self-calibration of the camera was performed within the designated measurement field. This calibration involved capturing a sequence of images from various perspectives, including convergent, frontal, and oblique views, to ensure accurate alignment and measurement. Once the calibration was completed, the camera settings were fixed and remained unchanged throughout the data acquisition process. Next the image sequence used to derive the vertical deformations was acquired in conjunction with the load vehicle's test cycle.

Both the calibration and subsequent data acquisition were carried out with the camera operating in image sequence acquisition mode. During the load tests, the pre-calibrated camera was mounted on a stable tripod and aligned to focus on the measurement field (Figure 5). As there is no connection between the bridge and the camera tripod, vibrations or shocks caused by the load vehicle do not affect the camera's stability.

Figure 5. Measurement setup consisting of a consumer camera mounted on a stable tripod.

To enhance the validity of the results, the described procedure was repeated using two different lenses, resulting in two distinct datasets. These datasets were used to evaluate the internal accuracy of the vertical deformation measurements. The primary objective was to assess the repeatability of the measurements and identify potential systematic errors.

2.4 Validation Data Acquisition

The openLAB research bridge, as stated in Section 2.1, is equipped with a comprehensive array of conventional sensors, e.g. acceleration- and tilt-sensors (Figure 6). Among these, the data collected from the installed tiltmeters plays a crucial role in validating the results generated by the photogrammetric system. One of the sensors installed on the bridge is a high-precision digital inclinometer provided by Sisgeo, specifically the model 0S542HD0502. This sensor utilizes MEMS technology to measure inclination changes in real time. Its robust design and thermal stability make it particularly well-suited for geotechnical and structural monitoring applications. Additionally, its digital data transmission capability ensures seamless integration into monitoring systems

These tiltmeters are installed on spans 1 and 2, with one sensor per girder, resulting in a total of six sensors. They are depicted in Figure 6 by red markings and the label TIL. They are positioned 4 m away in both directions from the bridge pear located at axis 20 (Figure 6), approximately at the point where the bending moment under the structure's self-weight is zero. This location is chosen because it is where the highest tilt is expected to occur. As described in section 2.2, the measurement point field is attached to span 1, so the data from the tiltmeter located on this span are relevant for this publication.

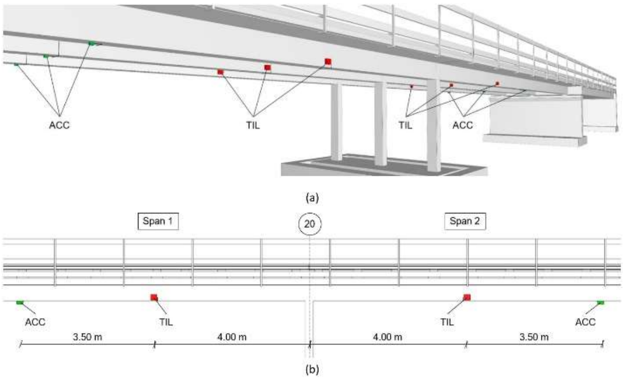

Figure 6. Sensor placement of the acceleration- (ACC) and tilt-sensors (TIL). Image source: (Jansen et al., 2025)

Jansen et al. (2025) shows that data acquisition from these sensors is carried out in two ways: For long-term studies, the sensors record data every 10 min. This involves measuring the tilt along the transverse bridge direction and the longitudinal bridge direction. The second data acquisition method is event-based and is controlled by threshold values accompanying the load tests. A 90 sec sample is acquired each time a load test is conducted with the load vehicle.

3. Photogrammetric Method

This section presents the method for conducting the preliminary computations required for camera calibration and determining the camera's external orientation of the monoscopic camera setup (Sec. 3.1), and for determining the primarily expected one-dimensional vertical deformation values (Sec. 3.2).

3.1 Data pre-Processing

The described measurement procedure produced two image sequences, each recorded at 30 frames per second (fps). The first sequence captured the measurement field under the calibration scheme (Figure 7, Cal), while the second sequence recorded the measurement field during the passage of the load vehicle, with the camera mounted on a tripod (Figure 7, Fix). Both sequences were subsequently decomposed into individual frames for further computation.

To perform the camera self-calibration, the image sequence must first be significantly reduced in number of images. There are two options for filtering the image data. As performing bundle adjustment with all images is too inefficient, one can either manually select the most convergent views of the measuring field from the calibration series, or automatically save every n-th image and only use those. Here the automatic reduced dataset is then used to determine 3D coordinates of the measurement field as well as the cameras external and internal orientation (IOR) parameters using Aicon 3D Studio. Additionally, one to three frames from the idle phase before the load vehicle starts of the second dataset are included in the bundle adjustment to estimate the external orientation (EOR) of the camera for the tripod-based measurement.

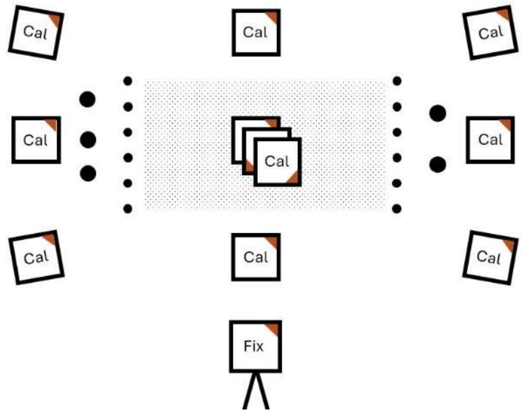

Figure 7. Schematic illustration of the calibration and measurement setup. Calibration images are labeled as “Cal” while the static sequence is denoted as “Fix”.

During the final preprocessing step, the image coordinates of the coded markers of the measurement field are measured in the frame sequence of the load vehicles passage. These were also determined using an ellipse-operator with subpixel accuracy in the Aicon 3D Studio software.

3.2 Calculation of vertical Deformation Values.

The vertical displacement values of the bridge superstructure are calculated according to the following pipeline:

1. Loading 3D coordinates, Camera-IOR, Camera-EOR and 2D image coordinates
2. Determine best-fit plane for measurement field points
3. Calculate distortion-corrected image coordinates
4. Calculation of image rays for the coded measurement points
5. Frame-wise intersection point calculation of image rays and best-fit plane
6. Vertical deformation component results from the difference to the first frame
7. Data smoothing and analysis

The initial step, after importing all the necessary data, involves determining the best-fit plane for the 3D coordinates of the measurement field prior to the load test. This is achieved using a standard MATLAB algorithm. As the main deformations are expected to affect the Z-direction, the best-fit plane calculated in the initial step is considered fixed throughout the entire load vehicle crossing.

In the subsequent step, the distortion correction of the image measurements is performed iteratively. Then, 3D image-rays of the distortion-corrected coded target image coordinate measurements are calculated for every frame of the sequence of the load test using the camera’s IOR and EOR. Firstly, the object coordinates XYZ^{i}_{world} of the image points are calculated using standard formulae (Eq. 1 and 2). Then, the vector from the projection center to each point $\overrightarrow{VEC}^i_{world}$ is determined (Eq. 3).

$$xyz^i_{cam} = \begin{bmatrix} x_{image} \\ y_{image} \\ c_{cam} \\ 1 \end{bmatrix}, \quad (1)$$

$$XYZ^i_{world} = M^0_{cam} * xyz^i_{cam}, \quad (2)$$

$$\overrightarrow{VEC}^i_{world} = \frac{XYZ^i_{world} - XYZ^0_{cam}}{\|XYZ^i_{world} - XYZ^0_{cam}\|}, \quad (3)$$

with: c_{cam} = focal length
x_{image}, y_{image} = image coordinates
M^0_{cam} = camera transformation matrix
XYZ^0_{cam} = camera projection center

In the second step, the intersection points $XYZ^i_{intersect}$ of the calculated vector and the best-fit plane of the measurement field are determined framewise (Eq. 4 and 5).

$$t^i = -\left(\frac{-\langle \vec{n}_{plane}, XYZ_{plane}\rangle + \langle \vec{n}_{plane}, XYZ^0_{cam}\rangle}{\langle \vec{n}_{plane}, \overrightarrow{VEC}^i_{world}\rangle}\right), \quad (4)$$

$$XYZ^i_{intersect} = XYZ^0_{cam} + \overrightarrow{VEC}^i_{world} * t^i, \quad (5)$$

with: $\vec{n}_{plane}$ = best-fit plane normal
XYZ_{plane} = best-fit plane points

Finally, the vertical bridge superstructure's displacement values d^i_{vert} are calculated for each frame in relation to a first (load free) frame $XYZ^0_{intersect}$ as follows (Eq. 6).

$$d^i_{vert} = XYZ^i_{intersect} - XYZ^0_{intersect}, \quad (6)$$

Since the measurement point field is aligned vertically on the bridge superstructure, the Z-component of the 3D intersection point $XYZ^i_{intersect}$ corresponds to the vertical deflection of the bridge superstructure d^i_{vert}. As the final step, a Gaussian weighted average filter is applied to the data to minimize measurement noise

4. Results and Discussion

4.1 Camera Calibration and EOR Determination

Since the calibration images were captured as an image sequence at 30 Hz, automatic reduction was selected to reduce the amount of data to be processed. To evaluate different levels of reduction, the image sequence for the dataset captured with the 35 mm lens was reduced to 50% of its original size, while the dataset of the 50 mm lens, was reduced to 10% of the initial image count. The first three images of the static sequence were then added. Figure 8 shows the positions of the static images marked with a red circle.

The accuracy values presented in Table 1 for the calculated bundle block adjustments highlight the limitations caused by the suboptimal configuration of the acquisition setup during the calibration sequence. To ensure a stable position for static image acquisition, the camera was set to an approximate object distance of 2 m for the 35 mm images and around 3 m for the 50 mm images.

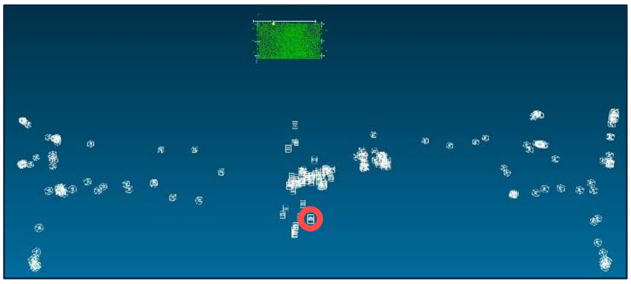

Figure 8. Camera image sequence for calibration- and additional frames for EOR-determination (red circle).

As the settings between calibration and data acquisition must remain stable, this configuration resulted in relatively low coverage of the image area by the measuring field in the calibration images. The convergent images also show lower degrees of tilting compared to those acquired with an optimal configuration. Overall, this results in an σ_0 of 1/9 pixel. The mean standard deviations of the calculated 3D coordinates of the measuring field are 0.03 mm for 35 mm images and 0.01 mm for 50 mm images. Note that the accuracy of camera calibration is not crucial here, as the results of data processing are short deformation vectors, with remaining systematic errors being highly correlated for start and end point of the vector.

	35 mm	50 mm
	mm	mm
σ_0	0.0013	0.0011
RMS_{σ_X}	0.030	0.016
RMS_{σ_Y}	0.023	0.011
RMS_{σ_Z}	0.037	0.014

Table 1. Results of the bundle adjustment

4.2 Vertical Displacement Values

The following chapter presents and analyzes the results of the vertical displacement measurements. To achieve this, the three static acquired image sequences were reduced by half, resulting in a frame rate of 15 Hz. The image coordinates of the measurement field were derived from the frame sequences corresponding to the three load vehicle test cycles. This process was carried out using Aicon 3D Studio software, which achieved an average internal precision of 0.15 µm (1/60 pixel) for the ellipse operator.

	35 mm		50 mm
	Cycle 1	Cycle 2	Cycle 3
	mm	mm	mm
$mRMS_{vert}$	0.014	0.007	0.009
$mSTD_{vert}$	0.012	0.005	0.007

Table 2. Mean standard deviation values of the raw values, averaged over all measurement points.

The mean measurement noise $mRMS_{vert}$ of the raw values, determined from images where the vehicle was stationary or at the starting point, averages approximately to 0.01 mm across all measurement cycles (Table 2).

To enable further analysis of the data, each data series for each measuring point was smoothed first. Figure 9 shows the resulting curves of the measurement points during a 90-second load test cycle. The measurement curves in this analysis are color-coded based on the load cycle. Each curve of a specific color corresponds to a single coded target point within the measurement field, as illustrated in Figure 4 from Section 2.2. The median is shown in yellow, derived across all individual measurement series of all three cycles.

The position of the load vehicle was not tracked externally during these investigations. However, based on a visual inspection of the frames, it is possible to determine the exact time at which the vehicle is directly above the measuring field. Using the dimensions of the bridge and the constant vehicle's speed of 4 km/h, it is possible to calculate the spatial position of the deflections of the measured value curve.

Figure 9 illustrates the symmetrical curve of deflection values, beginning at the starting point of the test vehicle at the beginning of bridge span 3. Five specific time points are highlighted and numbered in Figure 9, corresponding to distinct positions (1-5) of the load-vehicle during the test cycle. Visual frame analysis indicates that at position 2 and 4, the vehicle was directly above the measuring field in the middle of bridge span 1. On both the outward and return crossing, the load vehicle generated an average deflection of -1.7 mm.

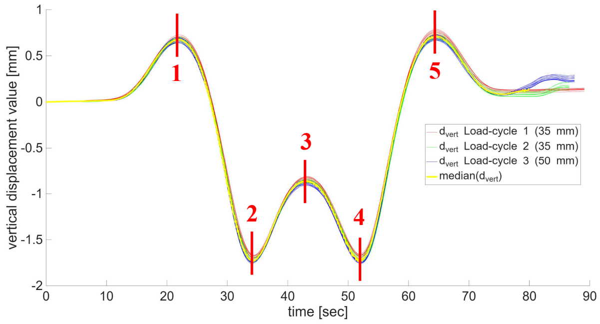

Figure 9. Frame-wise vertical displacement for load test cycles 1-3 (each comprising a forward and a backward traversal), the median over all cycles and five designated load vehicle positions (1-5).

Between these two points in time, the vehicle reached its end position (3) at the end of bridge span 1. This led to a 49.5 % reduction in deflection down to -0.86 mm. According to the bridge dimensions and the constant speed of the load vehicle, it was located approximately 5.6 m away from bridge span 3 on bridge span 2 which causes the deflection at position 1 and 5. Since span 2 and 1 are connected, this leads to a positive average deflection of 0.68 mm for the measuring points on the outbound passage and 0.72 mm on the return passage.

POI	$min(d^i_{vert})$	$max(d^i_{vert})$	$mean(d^i_{vert})$	$\Delta(d^i_{vert})$
sec	mm	mm	mm	mm
22	0.64	0.73	0.68	0.09
34	-1.76	-1.66	-1.71	0.10
43	-0.91	-0.81	-0.86	0.10
52	-1.76	-1.66	-1.71	0.10
64.5	0.66	0.79	0.72	0.12

Table 3. Minimum, maximum, mean and delta vertical deflection values measured at five designated load vehicle positions.

Two distinct effects can be identified both visually in Figure 9 and through the mean vertical deflection values presented in Table 3. The average vertical deflection between position 1 and 5 differs by 0.04 mm, even though it should theoretically be identical. Conversely, an increasing spread of the data curves is evident as the measurement duration increases. This is particularly visible in the increase of the delta values $\Delta(d^i_{vert})$ in Table 3 by 33 %. The initial effect could be ascribed to material inertia, which leads to deformed areas not instantly reverting to their original state.

4.3 Data Validation

Due to the lack of directly measured reference data for the vertical deformation values determined here, such as deformation values measured by tachymetry, data evaluation has been carried out in two stages.

In a first step, the two independent measurement series, utilizing different camera configurations, used to enable the estimation of internal accuracy and repeatability. For this purpose, the data from Cycle 1 and 2 of the 35 mm configuration is checked against the independent Cycle 3 (50 mm). As demonstrated in Section 4.2, all three cycles exhibit nearly identical curve progressions with no statistically significant deviations, thereby confirming the high repeatability of the measurement procedure. Notwithstanding this overall consistency, the monotonically increasing trend observed in the delta values (Section 4.2) constitutes the sole statistically significant finding. A closer inspection of position 5 (Figure 10), which corresponds to the largest delta value, indicates that the observed discrepancy cannot be attributed to differences between the two camera configurations; rather, it originates from differences between cycle 1 and cycle 2 of the 35 mm measurement.

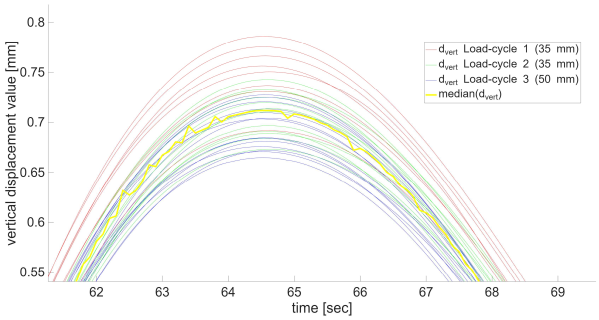

Figure 10. Detailed view of cycle 1 to 3 at position 5.

The observed systematic error may be attributed to several contributing factors. Varying atmospheric conditions – most notably intense solar irradiance – are considered a primary source, as they can induce thermal heating of the bridge structure and the camera system, potentially leading to thermally driven geometric instabilities in the imaging geometry. Furthermore, the self-weight of the camera may introduce a marginal, weight-related tilt of the camera-system, which likewise contributes to the systematic displacement trend identified in the photogrammetric displacement measurements.

The second part of the validation process involves using external reference data to examine the plausibility of the derived vertical displacement curve. In this subsequent stage, data from the tilt sensors (Jansen et al., 2025) is used to validate the load characteristics of the photogrammetrically detected deflection. For this purpose, the measurement data, used here, was averaged over the reference phase of the load tests. The analysis concentrated on the tilt sensor designated as G_TILX_P13_CB1100_0. This nomenclature encodes the designation of the measured value, as well as the sensor's position in relation to the structure. Here, TILX stands for the measured tilt along the bridge's longitudinal axis, while P13 specifies the sensor's installation location within the structure, corresponding to the precast element of span 1, girder 3. The measurement point field utilized in this study is positioned, as described in Section 2.2, at the center of the identical precast element. As outlined in section 2.4, the tiltmeter and the measurement point field are separated by a distance of 3.5 m. Figure 11 shows the averaged acquired tilt data of the bridge's superstructure in relation to the longitudinal axis of the bridge in mm/m.

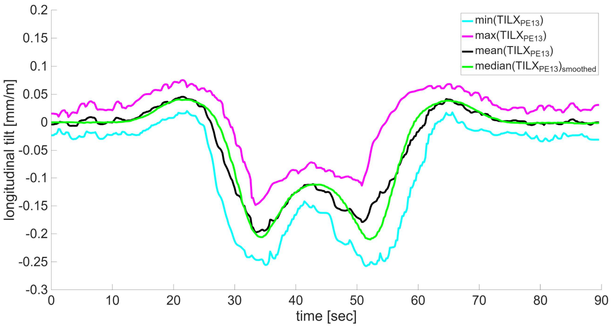

Figure 11. Averaged longitudinal tilt measurements of the reference phase from tilt sensor G_TILX_P13_CB1100_0.

As the two curves represent different measurement principles with differing units, the median-filtered value curves were normalized to be comparable. Figure 12 top shows the superimposed curves of the normalized, median-filtered values of the photogrammetrically determined vertical displacement and the longitudinal tilt values.

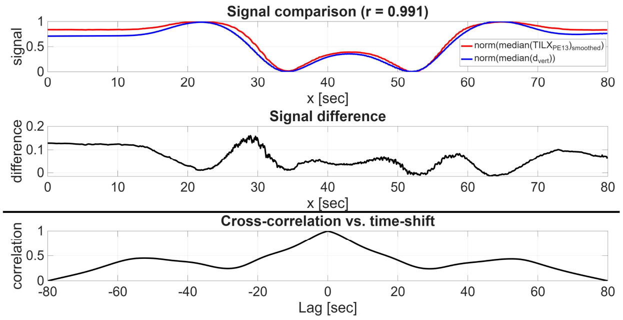

Figure 12. Normalized median displacement values and median tilt measurement data (top), signal difference (middle) and time-shift dependent cross-correlation (bottom).

The two curves clearly align, exhibiting the same overall progression. Notable differences, approximately 0.1, are observed only during the initial and final phases, specifically between the first maximum and first minimum (Figure 12, middle). The calculated cross-correlation value of 0.9915 confirms a strong similarity between the two measured curves. This high correlation is achieved without any time shift, as illustrated in Figure 12 bottom. Overall, both curves demonstrate the same characteristics of the bridge superstructure displacement.

5. Conclusion and Outlook

In this study, we demonstrated how a load-induced deformation of a bridge superstructure on a research bridge can be determined photogrammetrically. Since primarily a one-dimensional deformation in the vertical direction was expected, a monoscopic camera setup was chosen for the measurements. From the image sequences acquired with this setup, vertical displacements ranging from −1.7 mm to +0.7 mm were derived. The data, measured at a temporal frequency of 15 Hz, exhibited a mean measurement noise of 0.01 mm. Validation through comparison with an independent measurement series indicated a mean deviation of approximately 0.1 mm. The deformation profile, determined for a complete load test cycle comprising a forward and return passage, was validated using independently measured tilt data. A cross-correlation of the normalized measurement curves resulted in a correlation coefficient of 0.99. This demonstrates that the vertical deformation component can be determined using a monoscopic standard consumer-grade camera setup.

However, the method described here does not address all potential questions and, therefore, provides opportunities for adaptations in future investigations. For instance, a slight systematic drift is evident in the derived deformation profiles. This drift could potentially be attributed to the material inertia of the bridge or to thermal effects affecting both the structure and the camera. Future measurements could mitigate these effects through methodological enhancements. On the one hand, meteorological parameters at the camera's location should be recorded and jointly analyzed with data from sensors embedded in the research bridge to eliminate potential thermal influences. On the other hand, the existing network of measurement points could be extended by including additional stable control points located off the bridge, enabling an independent control for the camera position.

To obtain direct reference values for the determined deformations, additional measurements of bridge deformation values will be conducted alongside the image sequences acquisition using a geodetic total station or a laser tracker. The advantage of such an approach lies in the ability to obtain highly precise reference values for the vertical displacement, which are essential to assessing the absolute accuracy of the developed method.

Acknowledgement

This research project is funded by the German Research Foundation (DFG - 501724457) as part of the Priority Programme 100+.

References

Albert, J., Maas, H.-G., Schade, A., Schwarz, W., 2002. Pilot studies on photogrammetric bridge deformation measurement. *Proceedings of the 2nd IAG Commission IV Symposium on Geodesy for Geotechnical and Structural Engineering* 21, 24.

Benning, W., Lange, J., Schwermann, R., Effkemann, C., Görtz, S., 2004. Monitoring crack origin and evolution at concrete elements using photogrammetry. *ISPRS Congress Istanbul Commission* 2004.

Duran Vergara, L. C., Leicht, L., Beckmann, B., Maas, H.-G., 2025. Longitudinal wave propagation determination in concrete specimen under impact loading by ultrahigh-speed camera image sequence and strain gauge data analysis. *Measurement Science and Technology* 36(3), 035112.

Herbers, M., Richter, B., Bartels, J. H., Al-Zuriqat, T., Smarsly, K., Marx, S., 2024. openLAB–A large-scale demonstrator for advancing digital twin developments of bridges. *Proceedings of* *the ReConStruct: Resilient Concrete Structures, Proceedings of the 2024 fib Symposium*, 2057-2067.

IDA-KI, 2025. Automated assessment of monitoring data for infrastructure constructions, https://tu-dresden.de/bu/bauingenieurwesen/imb/forschung/Forschungsfelder/Ingenieurbau/digital-smart/IDA-KI. (Accessed 30 October, 2025)

Jansen, A., Herbers, M., Richter, B., Walker, M., Jesse, F., Marx, S., 2025. Monitoring data of the openLAB research bridge–Part 1: Reference condition. *Data in Brief*, 111624. doi.org/10.1016/j.dib.2025.111624

Kellner, M., Vassilev, H., Busch, A., Blaskow, R., Ferrandon Cervantes, M., Poku-Agyemang, K. N., ... & Blankenbach, J., 2024. Scan2BIM-A Review on the Automated Creation of Semantic-Aware Geometric as-is Models of Bridges. *Allgemeine Vermessungs-Nachrichten: AVN.*

Koschitzki, R., Schacht, G., Schneider, D., Marx, S., Maas, H.-G., 2011. Integration of photogrammetry and acoustic emission analysis for assessing concrete structures during loading tests. *Videometrics, Range Imaging, and Applications XI*, 8085, 198-205.

Liebold, F., Maas, H.-G., Deutsch, J., 2020. Photogrammetric determination of 3D crack opening vectors from 3D displacement fields. *ISPRS Journal of Photogrammetry and Remote Sensing*, 164, 1-10.

Maboudi, M., Backhaus, J., Mai, I., Ghassoun, Y., Khedar, Y., Lowke, D., ... & Gerke, M., 2025. Very high resolution bridge deformation monitoring using UAV-based photogrammetry. *Journal of Civil Structural Health Monitoring*, 1-20.

Marendić, A., Gajski, D., Duvnjak, I., Paar, R., 2025. Evaluation of Photogrammetric Methods for Displacement Measurement During Structural Load Testing. *Remote Sensing*, 17(15), 2569.